Eur. J. Mech. A/Solids 19 (2000) 31–50

Energy absorption of foam-filled circular tubes with braided composite walls

Anne-Marie Harte, Norman A. Fleck, Michael F. Ashby

Cambridge University Engineering Dept., Trumpington St., Cambridge, CB2 1PZ, UK

(Received 20 May 1999; accepted 14 October 1999)

Abstract – Braided glass-fibre/epoxy circular tubes with polymer foam cores are loaded in tension and in compression, and the energy of deformation is measured. Theoretical models of tube deformation are developed, and are used to predict the energy absorption as a function of tube wall strength, the ratio of tube wall thickness to tube diameter, and the density of the foam. The energy per unit mass and energy per unit volume are optimised with respect to the relative density and geometry. It is found that foam-filled braided circular tubes exhibit promising energy absorbing characteristics, due to a combination of energy absorption by the polymeric foam core and by the glass/epoxy braided tube. © 2000 Éditions scientifiques et médicales Elsevier SAS

braided composites / energy absorption / foam

1. Introduction

The design of air, sea and ground vehicles is increasingly driven by minimum weight considerations and by concerns for passenger safety. Composite structures are lightweight, can be tailored in composition and shape, and can provide high crashworthiness when used as part of an energy dissipating device, such as the sub-floor assembly of helicopter cabins, Cronkhite (1984). Braided composite tubes offer better energy-management characteristics than laminated composites because the intertwining fibre architecture prevents gross delamination, as discussed by Hamada et al. (1994). Further performance gain is achieved by filling the tubes with crushable foam.

Ideal energy absorbers have a long, flat load-deflection curve: the absorber collapses plastically at a constant force called the 'plateau force' F_{pl}, as sketched in *figure 1a*. Energy absorbers for crash protection and for packaging are chosen so that the plateau force is just below that which will cause damage to the protected object; the best choice is the one which has the longest plateau (i.e. the largest value of lock-up displacement u^*), and therefore absorbs the most energy. Solid sections do not perform well in this role. Hollow tubes, shells and metal honeycombs (loaded parallel to the axis of the hexagonal cells) have the appropriate shape of load-deflection curve; so, too, do foams.

Practical energy absorbers have a characteristic load-deflection response as sketched in *figure 1b*. An initial (or subsequent) peak value of load $F_{\max}$ exceeds the average value F_{av}, and leads to an increased acceleration and potential damage to the object. The 'crush force efficiency', defined by $\eta = F_{\text{av}}/F_{\max}$, is a useful measure of the uniformity of collapse load; for the ideal energy absorber, $\eta = 1$. The crush force efficiency is closely related to the structural effectiveness introduced by Puglsey (1960), defined as the ratio of the average collapse load to the limit load of the structure. In the ideal case, an energy absorber is also as compact as possible, with a length L equal to the useful stroke length u^*; in practice, the 'stroke efficiency', SE, defined by $\text{SE} = u^*/L$ is less than unity. In summary, crashworthiness is maximised by using an energy absorber of high crush force efficiency, and of high stroke efficiency. In energy absorption applications a typical design requirement is to use

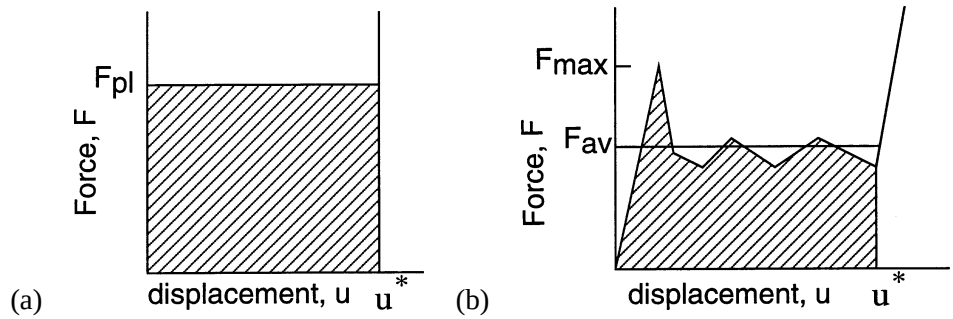

Figure 1. (a) The force-deflection characteristic of an ideal energy absorber; (b) Typical force-deflection characteristic of a practical energy absorber.

an energy absorbing device of minimum volume or of minimum mass for a given level of absorbed energy W, and for a peak collapse force $F_{\max}$. In this study, the uniaxial compressive and tensile behaviour of braided glass-fibre/epoxy circular tubes containing a polymeric foam core are examined theoretically and experimentally, and their potential as energy absorbers is explored.

The structure of this paper is as follows. First, measurements and models are reviewed for the axial crushing of empty and foam-filled circular tubes; collapse is by a number of competing deformation modes, including tube inversion, progressive pulverisation and buckling. Second, an experimental program is reported on the compressive and tensile behaviour of foam-filled glass/epoxy braided tubes. The foam core raises the level of energy absorption: in the compression tests the foam crushes axially, whereas in the tension tests, the foam core undergoes radial crushing due to a reduction of the braid diameter as it extends. Motivated by these experiments, simple analytical models are derived for the energy absorbed in tension and in compression, and the predictions are compared with the measured values. In order to explore the potential of foam-filled tubes for energy absorption, the predicted energy per unit mass and energy per unit volume are optimised with respect to the relative density of the foam, and with respect to the strength and geometry of the braided tube.

2. Previous work on the compressive crushing of tubes

Circular cylindrical structures deform in compression by at least four competing mechanisms: (i) tube inversion, (ii) progressive crushing, (iii) axisymmetric buckling and (iv) diamond-shape buckling. These four modes are depicted in *figure 2*, and are summarised as follows.

2.1. Tube inversion (figure 2a)

Tube inversion involves the bending and stretching of a tube to a larger or smaller diameter. An end fixture is needed to trigger and maintain this deformation mode, and this adds weight to the energy absorbing system (Barrett, 1996). The large plastic strains involved in tube inversion limit its occurrence to ductile materials, such as steels and aluminium alloys, and to braided and filament wound composites, as observed recently by Harte (1997). The steady state inversion of metallic tubes has been analysed by Al-Hassani et al. (1972) via a plastic work calculation.

2.2. Progressive crushing or pulverisation (figure 2b)

Progressive crushing is a commonly observed failure mode for composite tubes in compression (Hull, 1983; Kindervater and Georgi, 1993; Haug and De Rouvray, 1993). When this mode of failure is desired, the ends

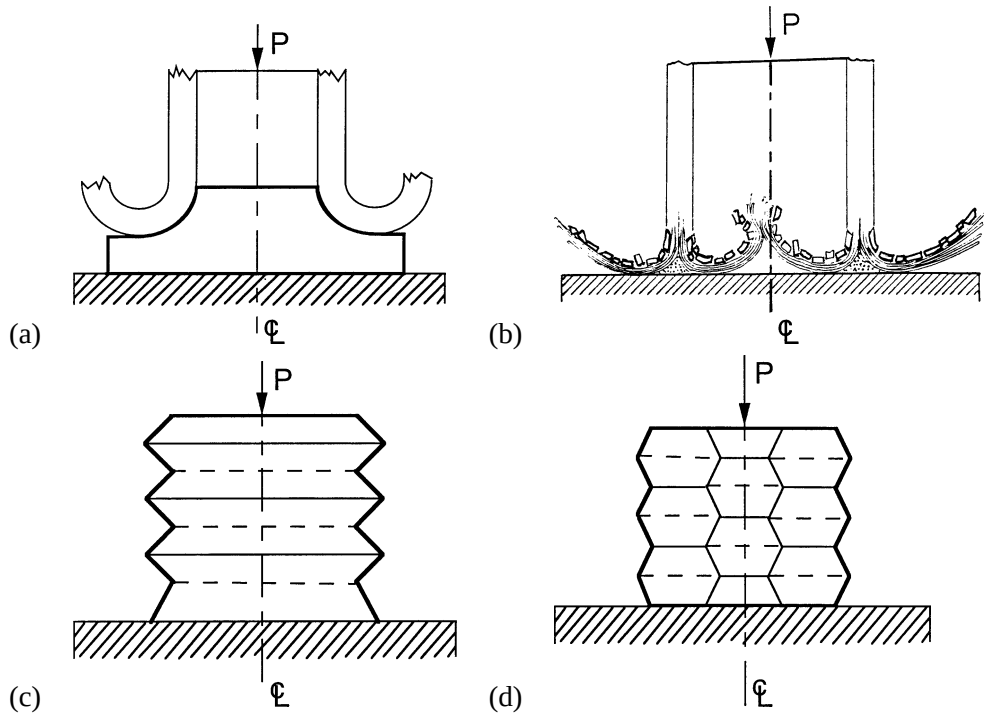

Figure 2. Axial modes of collapse for cylinders: (a) tube inversion; (b) progressive crushing; (c) axisymmetric buckling, and (d) diamond buckling.

of the tube are usually chamfered to trigger the failure. The high energy absorption is associated with the large number of microfractures that occur as the tube crushes; energy dissipation results from the generation of fracture surface area, from friction between fragments, and from plastic shear of the matrix.

Chiu et al. (1998) have recently explored this failure mode for biaxial and triaxial braids: the effect of fibre orientation upon the collapse response was measured for carbon/epoxy braids of fibre lay-up $(\pm\theta/0°)$. One end of the specimens was chamfered, and consequently the specimens failed by a progressive splaying mode of crushing; the average width of the splaying fronds increased with increasing braid angle but decreased with increasing axial yarn content.

2.3. Axisymmetric buckling and diamond shaped buckling (figures 2c and d)

Elastic shells fail by a number of buckling modes, as depicted in *figures 2c* and *2d*, and as reviewed by Timoshenko and Gere (1961). In general, classical elastic bifurcation analysis fails to predict the peak load observed in practice: for example, the observed buckling load of circular aluminium tubes is typically one third of the bifurcation load (Weingarten et al., 1968). In order to predict realistic buckling loads, the effects of material non-linearity and geometric imperfections must be included, see for example Hutchinson (1974).

The ratio of tube wall thickness to tube radius is the dominant factor in determining whether axisymmetric buckling or diamond buckling will occur in both elastic and plastic buckling: thick isotropic tubes fail by axisymmetric buckling, whereas thin-walled tubes fail by diamond buckling (Mikkelsen, 1999; Tvergaard, 1983). For geometries close to the transition, a specimen can switch from one mode to another during a single test (Andrews et al., 1983).

Large plastic strains accumulate in the plastic hinges for both axisymmetric and diamond buckling, and so fibre composite tubes fail by this mode only when the matrix and fibres possess high failure strains. Thornton (1979) found that Kevlar/epoxy tubes of orientation $\pm 45^\circ$ collapsed by diamond buckling, whereas tubes of $0^\circ/90^\circ$ lay-up (with reduced axial and circumferential ductility) failed by end fragmentation. Karbhari et al. (1997) have observed axisymmetric and diamond buckling of hollow circular tubes made from $\pm 45^\circ/0^\circ$ triaxial braids, with fibres of glass, Kevlar and carbon in a vinyl ester resin. They found that the highest energy absorption was obtained using glass-carbon and Kevlar-carbon fibre hybrids, with the carbon fibres comprising the axial yarns of triaxial braids.

A number of investigators have developed approximate models for the post-buckling collapse of metallic and polymeric tubes by both axisymmetric buckling and diamond buckling, including Pugsley and Macaulay (1960), Alexander (1960), Johnson et al. (1977), and Mamalis et al. (1986, 1989). Pugsley and Macaulay (1960) estimated the mean load for plastic diamond buckling of a rigid, ideally plastic solid. They split the energy absorbed into two parts: (i) plastic bending at the edges of the folded plates, and (ii) plastic stretching as the original square plates deform into rhomboids. The total plastic work is equated to the work done by an external load. Their theory compared well with experimental measurements of the average collapse stress for stainless steel and aluminium circular cylinders.

Alexander (1960) addressed axisymmetric buckling, and he also used a plastic work calculation to estimate the average collapse load. He equated the external work to the internal work associated with the plastic bending of circumferential hinges and with axisymmetric stretching. Minimisation of the average collapse load with respect to the buckle wavelength gave an expression for the wavelength. Alexander found that the buckle wavelength is approximately equal to $\sqrt{Dt}$, where D is the tube diameter and t is the wall thickness. This wavelength is slightly less than the value given by Timoshenko and Gere (1961) for elastic buckling. Recently, Mikkelsen (1999) has found that Alexander's approximation for the buckle wavelength is in good agreement with that found by a full numerical analysis of axisymmetric plastic buckling.

Johnson et al. (1977) extended the ideas of Alexander (1960) and Pugsley and Macaulay (1960) by proposing two types of collapse mode: the plastic hinges are taken to be either stationary or moving. In the simpler stationary hinge case, the plastic work is partitioned into the work needed to bend the material at the hinges and the work needed to flatten the initially curved triangular or trapezoidal segments into flat plates. Their more complex but more accurate solution was obtained using 'travelling hinges', wherein the plastic hinges are assumed to propagate along the axis of the specimen. The accuracy of this solution was verified by Mamalis et al. (1989) in a series of experiments on the crushing behaviour of grooved PVC tubes.

Wierzbicki et al. (1992) have described axisymmetric buckle propagation by the sequential formation of an active crush zone along the length of the tube. The tube crumples within the active crush zone, and after lock-up of the active zone occurs, an adjacent crush zone forms and the cycle is repeated. Two levels of approximation of geometry of crush zone are made: a simplified geometry, wherein prismatic straight elements rotate about stationery hinges, and a more sophisticated model comprising two S-shaped 'superfolding elements'. For both geometries, closed form solutions were obtained for the average load and the buckle wavelength. Both models succeeded in describing aspects of the observed behaviour not captured hitherto: alternating heights of peaks in the load-displacement curve, an unequal distance between peaks, a reduced crush distance and a realistic shape of crushed tubes. The more complex crush zone geometry led to more accurate predictions than the simpler stationary hinge model.

Experimental and theoretical evidence are accruing that the average force necessary to collapse a foam filled tube is greater than the sum of the collapse force of an empty tube and the foam individually. Abramowicz and Wierzbicki (1988) coupled the response of a foam core to that of a metallic tube and concluded that the stiffening effect of the foam decreases the buckle wavelength, and increases the amount of absorbed energy

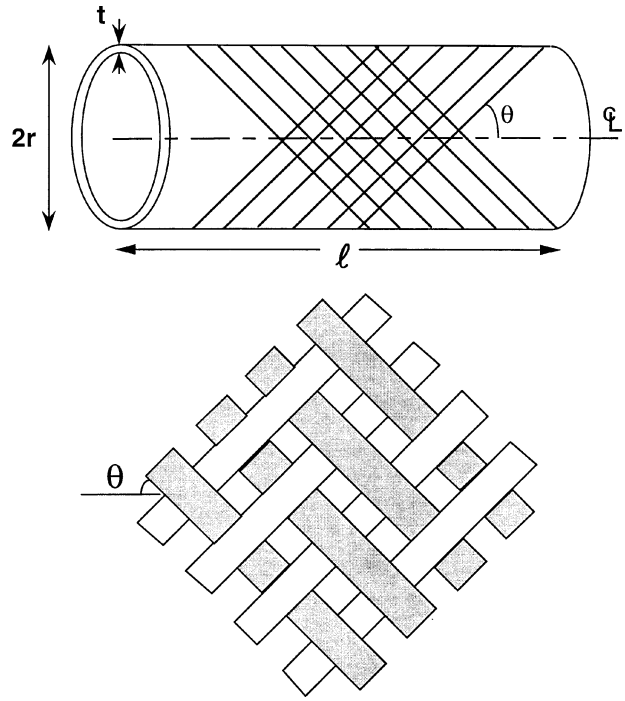

Figure 3. Geometry of a foam-filled braided tube.

within the tube. Reid et al. (1986) have treated the foam-filled structure as an elastic plate on an elastic foundation to find the reduced buckle wavelength. This value of wavelength is used to calculate the separate contributions to absorbed energy from the tube and the polyurethane foam. Langseth et al. (1998) and Hanssen et al. (1999) observed a reduction of buckle wavelength when crushing square aluminium extrusions with an aluminium foam filler. Hanssen et al. (1999) found that the elevation in collapse force associated with the interaction between foam and tube is described accurately by an empirical non-dimensional function of the foam plateau stress, the flow strength of the tube wall, the tube width and the wall thickness.

3. Experimental program

Exploratory tension and compression tests have been performed on glass/epoxy braided tubes containing a polymeric foam core. These experiments are used to motivate simple models of tube deformation.

3.1. Compression of foam-filled braided tubes

Braided tubes were manufactured manually using a Maypole braiding machine, such that the tube wall comprises a single layer of $\pm\theta$ 2-over, 2-under regular braid with 32 tows in the $+\theta$ direction and 32 tows in the $-\theta$ direction, see *figure 3*. Each tow consists of approximately 1 600 glass fibres. The matrix is a two part casting epoxy under the tradename of Ciba Geigy Araldite MY 753; it is a plasticised liquid epoxy resin with hardener HY 956, mixed 100 parts to 20 parts by volume. After hand-brushing of the epoxy onto the tows, the epoxy wicked between individual fibres. The samples were cured in an air oven at 100 °C for 20 min. After curing, the braided tubes were cut so that their length was approximately equal to their diameter, and the ends

Table I. Material properties of the braided tubes and foams used in axial compression and tension tests.

Braided tube properties					
	Radius r (mm)	Wall thickness t (mm)	Tube wall yield strength Y (MPa)	Shear strength of epoxy τ_Y (MPa)	Density of tube wall ρ_t (Mg/m^3)
$\theta_0 = 40°$	21.1	0.98	60	22	1.8
$\theta_0 = 55°$	26.5	0.93	25	22	1.8

Foam properties			
	Strength of cell wall σ_c (MPa)	Density of foam ρ_f (Mg/m^3)	Density of cell wall material ρ_s (Mg/m^3)
Polyurethane	127	0.16	1.2
Polymethyl-acrylamid	120	0.08	1.3

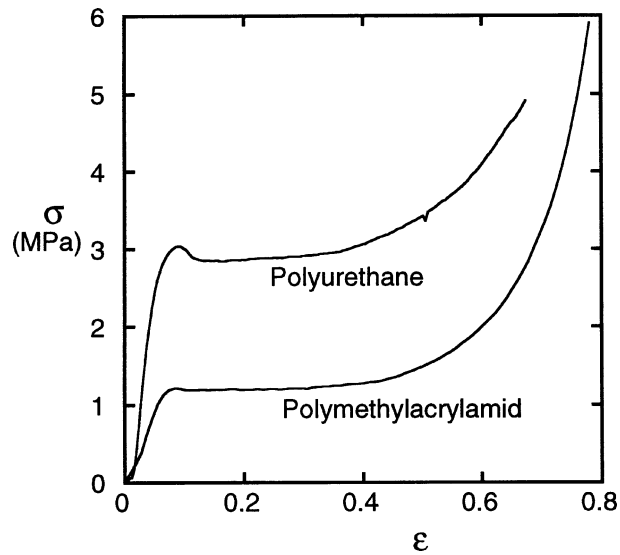

Figure 4. The nominal stress versus nominal strain responses of polyurethane foam ($\rho_f = 160$ kg/m^3) and polymethyl-acrylamid foam ($\rho_f = 80$ kg/m^3) in compression. The nominal strain rate $\dot{\varepsilon}$ equals 1.2×10^{-4} s^{-1}.

of each circular tube were turned on a lathe to ensure that the end faces were perpendicular to the specimen axis. The tubes were of diameter 42.2 mm, of length 46 mm and of wall thickness 0.93 mm. The specimen geometry and braid unit cell are sketched in *figure 3*, and are listed in *table I*.

Two closed cell polymeric foams were used as cores: a rigid polyurethane foam of density 160 kg/m^3 supplied by Kooltherm Insulation, and a polymethyl-acrylamid foam of density 80 kg/m^3, known as Rohacell. The nominal stress versus nominal strain curve for each foam in compression is shown in *figure 4*, for a strain rate of 1.2×10^{-4} s^{-1}. The expected collapse response is displayed: linear elastic, followed by a plateau region and then final lock-up. Pertinent materials properties of the foams are included in *table I*.

The foam cores were machined to a sliding fit inside the braided tubes and were inserted without adhesive. The foam-filled tubes were then loaded to failure in uniaxial compression at a nominal strain rate of 6.0×10^{-4} s^{-1}, using a screw-driven test machine and parallel loading platens which had been lubricated with

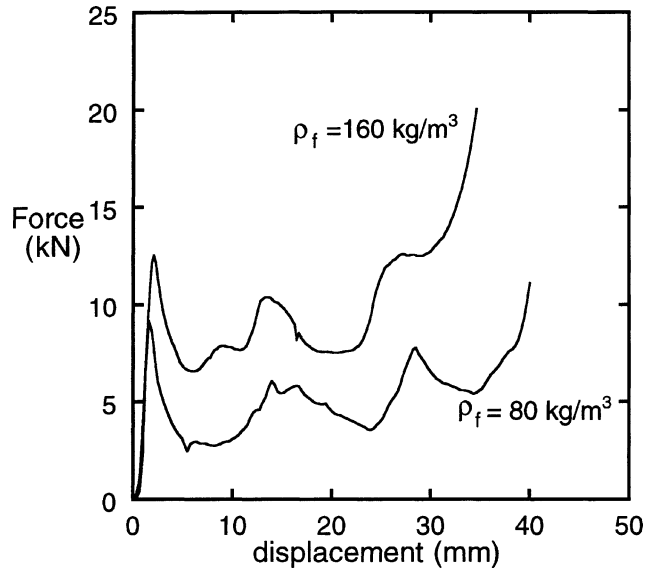

Figure 5. Load versus displacement curves for uniaxial compression of braided tubes with foam cores. The foam of density 160 kg/m^3 is made from polyurethane, whereas the foam of density 80 kg/m^3 is made from polymethyl-acrylamid. For both foam-filled tubes, the initial helix angle $\theta_0 = 40°$ and $r/t = 23.4$.

Table II. Measured crashworthiness parameters for the axial crushing of foam-filled braided circular tubes.

	Specific energy (kJ/kg)	Mean crushing stress (MPa)	Crush force efficiency	Stroke efficiency
$\theta_0 = 40°$, polyurethane core	14.5	6.38	0.77	0.73
$\theta_0 = 40°$, polymethyl-acrylamid core	9.08	3.29	0.55	0.85

PTFE spray. *Figure 5* shows the load versus shortening curves for the glass/epoxy braided tubes containing a rigid polyurethane core (density, $\rho_f = 160$ kg/m^3), and a polymethyl-acrylamid core ($\rho_f = 80$ kg/m^3). The radius-to-wall-thickness ratio r/t for these tubes equals 23.4, and the initial helix angle θ_0 equals 40°. *Table II* gives the corresponding measures of crashworthiness: the energy absorbed per unit mass, the stroke efficiency and the crush force efficiency, as defined in the Introduction. Collapse is by axisymmetric buckling, as shown in *figure 6* for a sectioned specimen containing a polyurethane foam core.

3.2. Tension of foam-filled braided tubes

Tensile stress–strain curves were measured for glass fibre braids containing no matrix (referred to as a 'dry braid') and for two glass fibre/epoxy braids. All specimens contained an unbonded polyurethane foam core, of density 160 kg/m^3, and were subjected to uniaxial tension using a screw driven test machine, at a nominal strain rate $\dot{\varepsilon}$ of 1.2×10^{-4} s^{-1}. Epoxy adhesive in combination with jubilee clips were used to fasten the specimens to circular cylindrical grips. The length of each specimen was about four times its diameter.

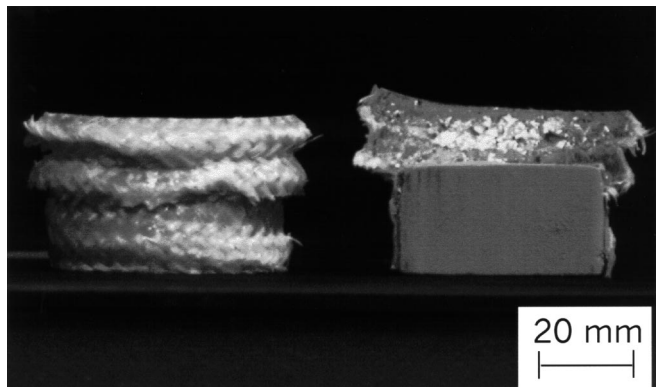

Figure 6. Cross-sectioned braided tube with polyurethane core after uniaxial compression. $\theta_0 = 40°$.

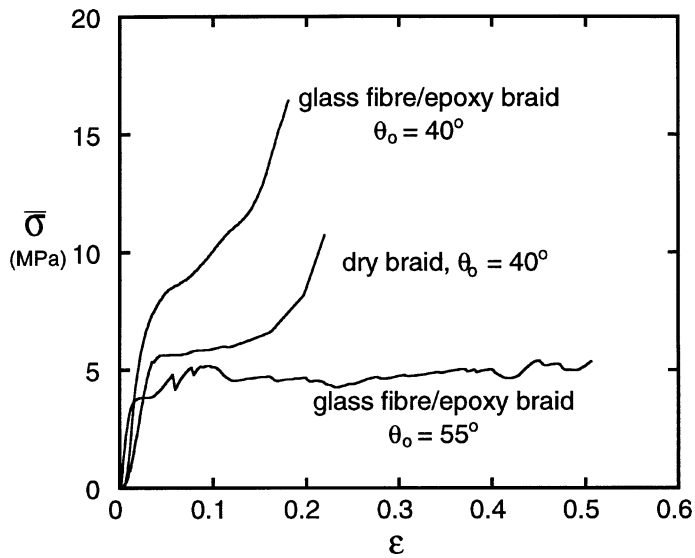

Figure 7. Tensile nominal stress versus nominal strain curve for three braids with polyurethane foam cores of density 160 kg/m^3. $\overline{\sigma}$ is the average stress over the cross section of the braided tube and foam core. (i) A dry braid with $\theta_0 = 40°$, $r/t = 23.3$; (ii) a glass fibre/epoxy matrix braid with $\theta_0 = 55°$, $r/t = 28.7$, and (iii) a glass fibre/epoxy matrix braid with $\theta_0 = 40°$, $r/t = 23.3$.

The nominal stress versus nominal strain response for a dry glass braid (no matrix) containing the polyurethane core is shown in *figure 7*. Here, the nominal stress is defined by the axial load divided by the initial cross-sectional area of the tube, and is to be distinguished from the axial stress on the tube wall. The initial helix angle θ_0 is 40° and the ratio of radius to wall thickness r/t is 23.3. Glass/epoxy braids with foam cores were also tested for the two helix angles, $\theta_0 = 40°$ and 55°, and the results are included in *figure 7*. The ratio of radius to wall thickness is $r/t = 23.3$ for $\theta_0 = 40°$ and $r/t = 28.7$ for $\theta_0 = 55°$. It is seen immediately from a comparison of the load versus displacement curves in compression (*figure 5*) that a pronounced load peak occurs in compression but not in tension. The presence of this load peak reduces the crashworthiness of the structure, as it leads to an increased acceleration rate of the crashed body: the crush force efficiency $\eta \equiv F_{\text{av}}/F_{\text{max}}$ is reduced.

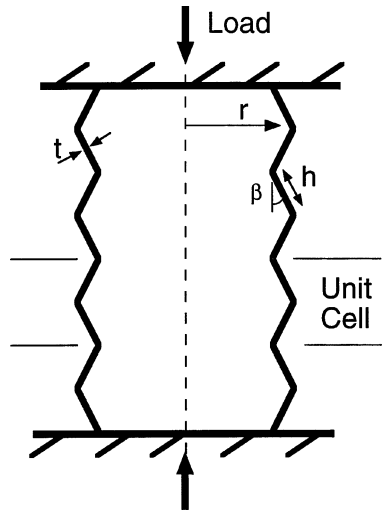

Figure 8. Progressive collapse by axisymmetric buckling.

4. An analytical model for energy absorption of foam-filled braided circular tubes in compression

In this section, we estimate the energy absorbed by a foam-filled braided tube in compression. To do so we adapt the methods of Reddy and Wall (1988) and of Alexander (1960): we split the energy absorbed by a tube when it undergoes axisymmetric buckling into the energy required to bend the material at the circumferential hinges through an angle of 2β and the energy required to stretch the material circumferentially between the hinges, see *figure 8*. A simple plastic work calculation is performed and for this purpose the braid is treated as a rigid-ideally plastic solid. Following preliminary observations of the buckling mode of the foam-filled braided tubes as evidenced in *figure 6*, it is assumed that the unbonded foam core prevents the braided tube from collapsing radially inwards, but does allow for free radial expansion of the tube. (This is in contrast to the observations of Hanssen et al. (1999) on aluminium tubes with aluminium foam cores: they found that the foam is radially crushed by the tube wall.) In our tests, the final hinge angle β^* after collapse is fixed by the final crushing strain of the foam, or by contact between the adjacent folds of the tube walls. The average axial force on the foam-filled tube is found by equating the total energy absorbed in deforming the foam core and the tube to the work done by the external load. The details are as follows.

The work done in axisymmetrically folding a tube into a concertina shape is split into two parts: that required to fold the material at the hinges and that required to stretch the material between the hinges. We shall calculate each contribution in turn. Consider the incremental plastic collapse of a representative unit cell by the rotation of a pair of straight-sided annular segments of the tube wall, see *figure 8*. Each segment has rotated by $\pm\beta$, and each hinge has rotated by 2β. The average circumferential length of each hinge equals $\pi(2r + h\sin\beta)$, where r is the tube radius, and h is the buckle length. The work increment $\mathrm{d}W$ in rotating the three hinges within the unit cell is

$$\mathrm{d}W = 4\pi(2r + h\sin\beta)M_\mathrm{p}\,\mathrm{d}\beta. \tag{1}$$

Upon assuming that the material is rigid-ideally plastic, the plastic bending moment per unit length M_p is given by $Yt^2/4$, where Y is the uniaxial yield strength of the tube wall in tension and in compression, and t is the wall thickness. Independent uniaxial tests on the glass/epoxy braids show that they behave in an elastic-plastic ductile manner, with an axial yield strength in tension equal to that in compression; the micromechanism of plastic flow is shear yielding within the epoxy matrix (Harte, 1997).

As mentioned above, the foam provides a unilateral radial constraint so that the tube can fold radially outwards but not inwards. Hence, the material must stretch circumferentially to accommodate buckling. This prevents diamond buckling by eliminating the compressive hoop stresses required for the initiation of diamond buckling (Mikkelsen, 1999; Harte and Fleck, 1999a). In the experiments on foam-filled composite tubes, the initial fibre orientation $\theta_0 = 40^\circ$ is close to an angle of 45°, and so we make the additional approximation that the composite behaves in a transversely isotropic manner, with the circumferential strength of the braided tube equal to the axial strength.

The work increment in hoop stretching two annular segments within the unit cell shown in *figure 8* is given by

$$\mathrm{d}W = 2\pi Y h^2 t \cos\beta \,\mathrm{d}\beta. \tag{2}$$

Thus, the total internal work in developing a single fold is calculated by integrating (1) and (2) from $\beta = 0$ to a final angle β^* which is specified below. On noting that the final nominal axial strain ε^* of the folded portion of the tube is related to the final angle β^* by

$$\varepsilon^* = 1 - \cos\beta^* \tag{3}$$

the external work in collapse of the unit cell of initial length $2h$ is $2\overline{P}h\varepsilon^* = 2\overline{P}h(1-\cos\beta^*)$ in terms of the average force $\overline{P}$. An energy balance of external and internal work gives

$$\overline{P} = \frac{\pi}{2} Y t^2 \left[1 + \frac{2r}{h}\frac{\beta^*}{1-\cos\beta^*}\right] + \pi Y h t \frac{\sin\beta^*}{1-\cos\beta^*} \tag{4a}$$

and, following Alexander (1960), we assume that wavelength h is such to minimise $\overline{P}$, giving $h = \sqrt{2rt}$ and

$$\overline{P} = \frac{\pi}{2}\left[\frac{(\beta^* + 2\sin\beta^*)}{1-\cos\beta^*}\sqrt{\frac{2r}{t}} + 1\right] Y t^2. \tag{4b}$$

The lock-up axial strain in the folded portion of the tube ε^* is limited either by the densification strain of the foam or by contact between the adjacent folds of the tube walls. Gibson and Ashby (1997) approximate the nominal axial strain for foam densification ε_D by

$$\varepsilon_\mathrm{D} = 1 - 2\frac{\rho_\mathrm{f}}{\rho_\mathrm{s}}, \tag{5}$$

where ρ_f is the density of the foam, and ρ_s is the density of the solid cell wall material. But we must also consider the axial crushing strain ε_C of the tube associated with contact between successive folds. If no foam is present the hinge rotates through $\beta = 90^\circ$ and the final nominal strain of the tube ε_C is approximated by $\varepsilon_\mathrm{C} = 1 - t/h$ or, upon substituting $h \approx \sqrt{2rt}$, is given by

$$\varepsilon_\mathrm{C} = 1 - \sqrt{\frac{t}{2r}}. \tag{6}$$

It is assumed that the foam-filled braided tube collapses to a final axial strain ε^* which is given by the smaller value of the maximum crushing strain of the foam ε_D defined in (5) and the crushing strain of the tube ε_C defined in (6). The final fold angle β^* is related to ε^* via (3).

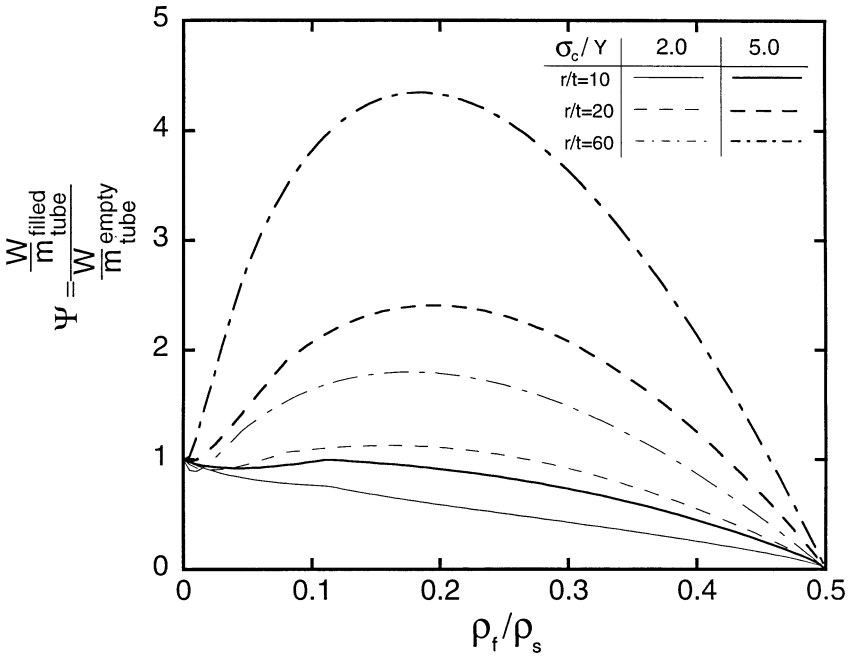

Figure 9. Normalised energy per unit mass of a foam-filled tube in compression, plotted against relative density of foam, for selected ratios of tube radius to wall thickness r/t, and of cell wall strength to tube wall strength, σ_c/Y.

The energy W absorbed by a length $\ell \gg h$ of the foam-filled tube combines the contributions from the foam and from the outer braided tube, to give

$$W = \left(\overline{P} + \pi r^2 \sigma_{pl}\right)\ell\varepsilon^*, \tag{7}$$

where the uniaxial crushing stress σ_{pl} of the foam is given by Gibson and Ashby (1997)

$$\sigma_{pl} = 0.3\sigma_c\left(\frac{\rho_f}{\rho_s}\right)^{3/2} \tag{8}$$

in terms of the crushing strength of the solid cell wall material σ_c. On noting that the combined mass of the tube and core m is

$$m = \left(\pi r^2 \rho_f + 2\pi r t \rho_t\right)\ell, \tag{9}$$

where ρ_t is the density of the tube material, the energy per unit mass W/m is obtained via (4) and (7)–(9) as

$$\frac{W}{m} = \frac{1}{2}\left(r^2\rho_f + 2rt\rho_t\right)^{-1}\left[\left(\frac{\beta^* + 2\sin\beta^*}{1-\cos\beta^*}\sqrt{\frac{2r}{t}} + 1\right)Yt^2 + 0.6\sigma_c\left(\frac{\rho_f}{\rho_s}\right)^{3/2} r^2\right]\varepsilon^*. \tag{10}$$

It is instructive to quantify the effect of a foam core upon the energy absorption by introducing the non-dimensional specific energy Ψ, defined by W/m for a filled tube normalised by W/m for an identical but empty tube (constrained against inward folding). *Figure 9* displays Ψ as a function of the relative foam density ρ_f/ρ_s for selected values of the ratio of wall radius to thickness r/t, and of the ratio of the foam cell wall crushing strength σ_c to the tube wall uniaxial yield strength, Y. Predictions are given for the representative measured

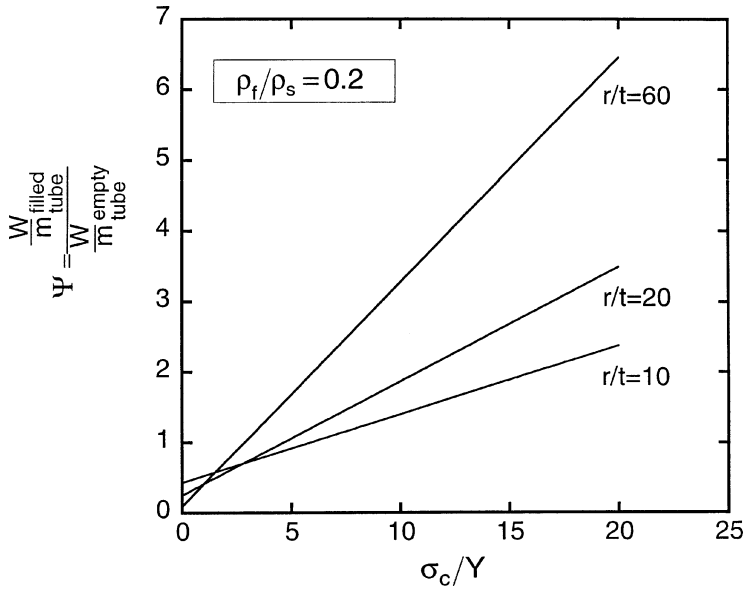

Figure 10. Plot of energy absorption in compression versus σ_c/Y for selected values of r/t, and $\rho_f/\rho_s = 0.2$.

value $\sigma_c/Y = 2$ (corresponding to a braided tube of helix angle $\theta_0 = 40°$, of uniaxial strength $Y = 60$ MPa, with a polymethyl-acrylamid foam core of cell wall strength $\sigma_c = 120$ MPa). For small values of r/t it is clear that the presence of the foam core does not increase the normalised specific energy Ψ. An optimal relative density of $\rho_f/\rho_s \approx 0.2$ exists such that Ψ is a maximum, regardless of the values of r/t and of σ_c/Y. In order to explore the dependence of the normalised energy Ψ upon r/t and σ_c/Y we plot Ψ against σ_c/Y in *figure 10* for selected values of r/t, with ρ_f/ρ_s held fixed at 0.2. It is clear from both *figures 9* and *10* that Ψ increases with both increasing σ_c/Y and r/t.

The predictions given by the above simplified theory may be compared with the experimental results presented in *figure 5* for a glass/epoxy braids and foam core. For the case where $\rho_f = 160$ kg/m^3, the predicted energy absorption is $W/m = 9.51$ kJ/kg, in satisfactory agreement with the measured value of $W/m = 14.5$ kJ/kg. Similarly, for the case $\rho_f = 80$ kg/m^3, the predicted energy absorption is $W/m = 8.22$ kJ/kg, in good agreement with the measured value of $W/m = 9.08$ kJ/kg. The predicted wavelength $\sqrt{2rt} = 7.1$ mm is in good agreement with the observed values of 7.6 mm and 7.9 mm for the tubes with a core of density 80 and 160 kg/m^3, respectively.

Material properties used in theoretical calculations of W/m are given in *table I* for all the foam-filled tubes used here. The yield strength of the tube wall Y was taken as the average of the strengths in a compression test and in a tension test on braided circular tubes (Harte, 1997); the strength of the foam cell wall material was found using the compressive data of *figure 4* and Eq. (8). The densities of the foam ρ_f and tube wall material ρ_t were measured directly and the densities of the cell wall materials ρ_s were manufacturers data.

The energy per unit mass is not the only relevant design parameter for energy absorption; the energy per unit volume is important where space is a limitation. Using a similar approach to that given above, the energy per unit volume W/V can be written

$$\frac{W}{V} = \frac{Y\varepsilon^*}{2}\left(\frac{t}{r}\right)^2\left\{\left(\frac{\beta^* + 2\sin\beta^*}{1-\cos\beta^*}\right)\sqrt{\frac{2r}{t}} + 1\right\} + 0.3\sigma_c\varepsilon^*\left(\frac{\rho_f}{\rho_s}\right)^{3/2}, \tag{11}$$

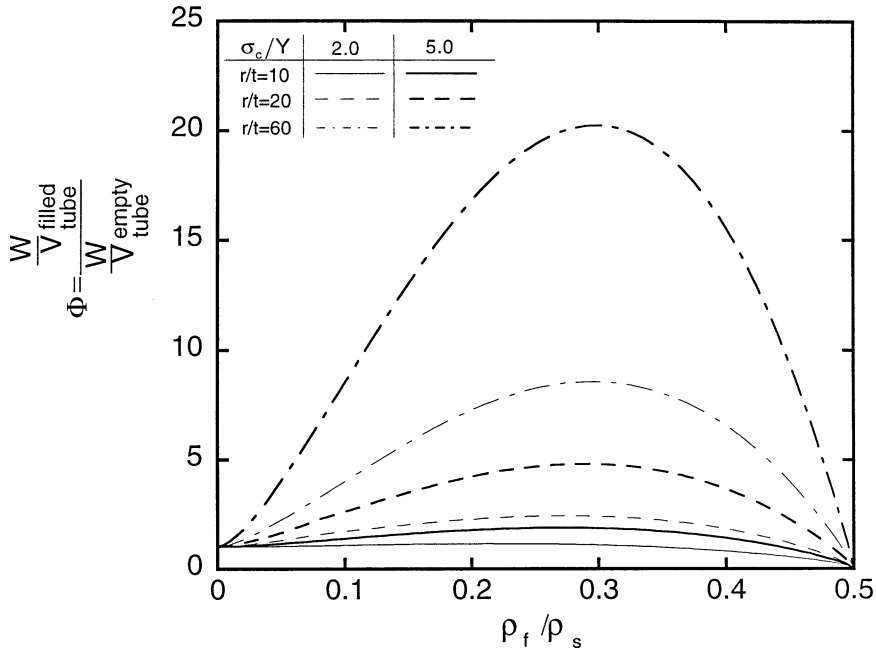

Figure 11. Normalised energy per unit volume in compression versus relative density ρ_f/ρ_s for selected values of radius to wall thickness ratio r/t, and foam cell wall strength to tube wall strength ratio, σ_c/Y.

where V is the enclosed volume of the tube in the initial state. We shall define Φ as the energy per unit volume for a filled tube, normalised by the value for an empty tube: it is an additional measure of structural efficiency, and is plotted against the relative density ρ_f/ρ_s of the foam core in *figure 11*, for selected values of σ_c/Y and r/t. As noted above for the normalised energy per unit mass of the foam-filled tube, an increase in σ_c/Y or r/t causes an increase in the energy per unit volume. The normalised energy per unit volume Φ is maximised at a foam relative density of about 0.3 for all values of σ_c/Y and r/t within the practical range. The maximum value of Φ is obtained within the regime where the final strain ε^* is associated with densification of the foam rather than lock-up of the braid. The switch in lock-up condition from that of the braid to that of the foam occurs at a relative density of 0.05–0.1 for the range of values of r/t considered in *figure 11*.

5. An analytical model for energy absorption of foam-filled braided circular tubes in tension

Most energy absorbing devices are used in compression, but there are some applications where energy absorption is required for tensile loading. In this section, an approximate analysis is performed to determine the energy absorbed by a foam-filled braided tube loaded in tension.

When a braided tube is pulled axially in tension the individual tows of the braid scissor, the length of the tube increases and its diameter decreases. A dry braid is unable to carry significant tensile load provided the tows are able to scissor freely. After some axial extension the tows lock-up, and the stiffness of the braid increases dramatically; dry braids lock-up at a braid angle such that the fibres in the tows and the tows in the braid are close-packed. The work of deformation (i.e. the energy absorbed) in extending the dry braid to lock-up is negligible. Significant energy can by absorbed by introducing a matrix into the weave of a tubular braid, or by introducing a foam core, or both. In order to predict the energy absorbed by a foam-filled fibre/matrix braid as the braid scissors through a large angle, the following micromechanical model is introduced.

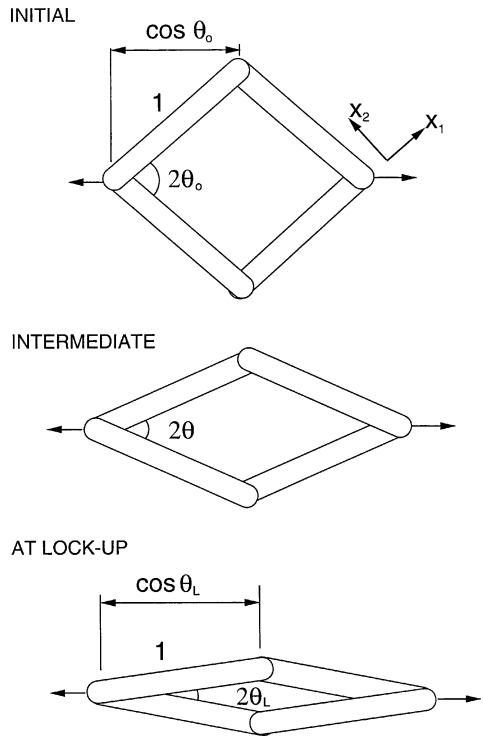

Figure 12. The kinematics of a braid in tension. The initial braid angle is θ_0, the current braid angle is θ and the lock-up angle is θ_L.

5.1. Kinematics of an empty braided tube in tension

The axial deformation of a braided composite tube is by the scissoring of tows past each other, from an initial angle θ_0 to a final angle θ^*. Post-failure microscopy of the glass/epoxy braids reveals that the pattern of microcracking within the matrix between the tows is accompanied on a smaller scale by microcracking of the matrix between individual fibres of each tow. This suggests that the kinematic description of scissoring of the tows also describes the relative motion of fibres within each tow. In the following analysis, we shall smear out the fibres and matrix, and define overall stress and strain measures for the smeared-out continuum.

It is convenient to calculate the strain rate within the composite in the reference frame of the rotating orthonormal axes (x_1, x_2), with the x_1-direction aligned with the fibres of orientation θ as shown in *figure 12*. The fibres in both the θ and the $-\theta$ directions are assumed to be inextensional; thus, in the (x_1, x_2) reference frame we have $\dot{\varepsilon}_{11} = 0$ and the strain rate components of interest are the strain rate transverse to the fibres $\dot{e}_t \equiv \dot{\varepsilon}_{22}$ and the shear strain rate $\dot{\gamma} = 2\dot{\varepsilon}_{12}$ along the fibre direction. In order to define $(\dot{e}_t, \dot{\gamma})$ we consider the relative velocities of neighbouring tows. The true transverse strain rate $\dot{e}_t$ is given by the separation velocity of the centre-lines of two neighbouring tows along the x_2-direction divided by their current separation,

$$\dot{e}_t = \frac{2}{\tan 2\theta}\dot{\theta}. \tag{12a}$$

The shear strain rate $\dot{\gamma}$ is defined by the rate of scissoring $2\dot{\theta}$ of fibres in the θ and the $-\theta$ directions, such that

$$\dot{\gamma} = 2\dot{\varepsilon}_{12} = -2\dot{\theta}. \tag{12b}$$

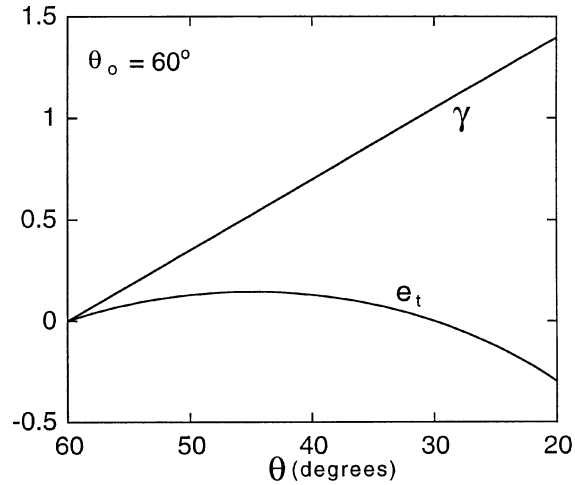

Figure 13. The evolution of transverse and shear strain in a braid for an initial helix angle of $\theta_0 = 60°$.

Integration from an initial helix angle θ_0 to a current angle θ gives

$$\gamma = 2(\theta_0 - \theta) \tag{13a}$$

and

$$e_t = \ln\left(\frac{\sin 2\theta}{\sin 2\theta_0}\right). \tag{13b}$$

The transverse and shear strains are sketched in *figure 13* for the case $\theta_0 = 60°$. As expected, the shear strain increases with decreasing helix angle θ. The transverse strain e_t reaches a maximum at $\theta = 45°$, then drops through zero to negative values with increasing θ. The negative transverse strains are associated with crumbling of the matrix from the braid. For an initial helix angle $\theta_0 > 45°$ the matrix shears and initially dilates under axial extension, whereas for $\theta_0 < 45°$ the matrix shears and initially compacts under axial extension. The distance between neighbouring tows and fibres reaches a maximum at $\theta = 45°$, at which point the matrix deforms in pure shear.

The ratio of current volume V to the initial volume $V_0 \equiv 2\pi r t \ell$ of the braid material is given by

$$\frac{V}{V_0} = \frac{\sin(2\theta)}{\sin(2\theta_0)} \tag{14}$$

and the internal energy dissipated in scissoring the fibres from $\theta = \theta_0$ to a final angle $\theta = \theta^*$ is

$$W = V_0 \int_0^{\gamma^*} \tau \frac{V}{V_0}\, \mathrm{d}\gamma + V_0 \int_0^{e_t^*} \sigma_t \frac{V}{V_0}\, \mathrm{d}e_t, \tag{15}$$

where $\gamma^* \equiv \gamma(\theta = \theta^*)$ and $e_t^* \equiv e_t(\theta = \theta^*)$ are given by (13), and τ and σ_t are the macroscopic shear stress and transverse stress in the current configuration, resolved onto the local fibre axes. The final braid angle θ^* is less than or equal to the lock-up angle θ_L of the braid: lock-up of the braid occurs at an angle θ_L for which the tows are tightly packed and can no longer scissor. Experiments show that θ_L is about 11° for a dry braid without a matrix and 21° for a braid with an epoxy matrix, regardless of the initial braid angle θ_0 (Harte and Fleck, 1999b).

On recalling that the scissoring of the braid is dictated by a single degree of freedom θ we can re-write (15) as

$$W = V_0 \int_{\theta_0}^{\theta^*} -\tau \frac{2\sin 2\theta}{\sin 2\theta_0}\,\mathrm{d}\theta + V_0 \int_{\theta_0}^{\theta^*} \sigma_\mathrm{t} \frac{2\cos 2\theta}{\sin 2\theta_0}\,\mathrm{d}\theta. \tag{16}$$

The axial strain of the braid ε_a is related to the current braid angle θ and to the initial braid angle θ_0 by

$$\varepsilon_\mathrm{a} = \frac{\cos\theta - \cos\theta_0}{\cos\theta_0}, \tag{17}$$

where $2\cos\theta_0$ is the original axial length of a braid unit cell and $2\cos\theta$ is the current length, see *figure 12*. By the same argument the circumferential and radial strains are expressed by

$$\varepsilon_\mathrm{r} = \frac{\sin\theta - \sin\theta_0}{\sin\theta_0}. \tag{18}$$

5.2. Energy dissipation in tensile deformation

Energy is dissipated in the foam-filled braid by plastic elongation of the braid and by radial crushing of the foam core. In order to obtain a closed form solution for the energy dissipated in tension, we simplify the integral (16) by assuming that the composite behaves as a rigid-ideally plastic solid, with the $+\theta$ layer yielding in shear at $|\tau| = \tau_Y$, and similarly for the $-\theta$ layer. Further, it is assumed that the presence of extensive microcracking within the matrix reduces the level of transverse stress σ_t to a negligible level. Consequently, we set $\tau = \tau_Y$ and drop the second term on the right hand side of (16).

Next, consider the energy dissipated within the foam core. It is assumed that the core is not bonded to the braided tube, and is subjected to equi-biaxial straining due to radial compression by the braid. The available experimental evidence suggests that polymer foams obey a maximum principal stress criterion for compressive yielding (Gibson and Ashby, 1997). We adopt the criterion that the densification strain under equi-biaxial straining equals that for uniaxial straining; this is consistent with the notion of independent plastic collapse in orthogonal directions, as suggested by a maximum principal stress criterion. Thus, the plastic work W_f dissipated in radially crushing a foam of length ℓ and area πr^2 by a radial strain ε_r^* is given by

$$W_\mathrm{f} = 2\pi r^2 \ell \sigma_\mathrm{pl} \varepsilon_\mathrm{r}^*, \tag{19}$$

where σ_pl is the plateau stress for the foam in uniaxial compression. The total energy dissipated by the foam filled tube is the sum of (19) and the integrated form of (16), to give

$$W = 2\pi \left(\frac{\cos 2\theta^* - \cos 2\theta_0}{\sin 2\theta_0} \right) r t \ell \tau_Y + 2\pi r^2 \ell \sigma_\mathrm{pl} \varepsilon_\mathrm{r}^*. \tag{20}$$

The specific energy absorbed by the foam-filled tube is obtained by dividing the total energy W by the mass as stated in (9), giving

$$\frac{W}{m} = \left(\rho_\mathrm{t} + \frac{r}{2t}\rho_\mathrm{f} \right)^{-1} \left[\left(\frac{\cos 2\theta^* - \cos 2\theta_0}{\sin 2\theta_0} \right) \tau_Y + \frac{r}{t} \sigma_\mathrm{pl} \varepsilon_\mathrm{r}^* \right], \tag{21}$$

where ε_r^* is the nominal radial strain at lock-up. It remains to specify the lock-up strain ε_r^* and the final angle θ^*.

Lock-up can occur first in the foam core or in the braided tube. We assume that the foam core locks-up when the radial strain ε_r attains the value ε_D, where ε_D is the uniaxial densification strain for the foam, and

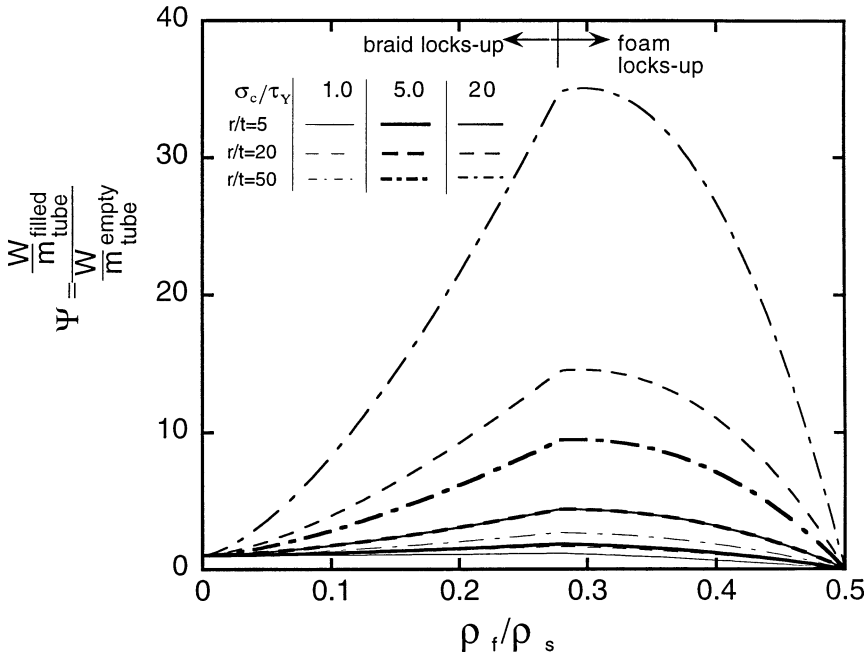

Figure 14. Normalised energy per unit mass of foam-filled tubes in tension, plotted against relative density of foam, for selected ratios of tube radius to wall thickness r/t, and crushing strength of the foam cell walls to matrix shear strength, σ_c/τ_Y.

depends upon the relative density ρ_f/ρ_s according to (5). The corresponding braid angle follows from (18) as $\theta^* = \arcsin[(1-\varepsilon_D)\sin\theta_0]$. Alternatively, the braid locks-up at an angle θ_L, as discussed above. When this limit is attained, we set $\theta^* = \theta_L$ and the corresponding radial strain in the foam core is given by $\varepsilon_r^* = (\sin\theta_L - \sin\theta_0)/\sin\theta_0$ from (18). The average axial nominal stress σ_a on the tube cross-section is obtained by equating the expression (20) for the internal work to extend a foam-filled tube to the axial lock-up strain ε_a^* to the external work,

$$W = \pi r^2 \ell \sigma_a \varepsilon_a^*, \tag{22}$$

giving,

$$\sigma_a = \left(\frac{\cos 2\theta^* - \cos 2\theta_0}{\sin 2\theta_0}\right)\frac{2t}{r}\frac{\tau_Y}{\varepsilon_a^*} + \frac{2\varepsilon_r^*}{\varepsilon_a^*}\sigma_{pl}. \tag{23}$$

It is instructive to plot the energy per unit mass of the foam filled tube, normalised by that of an empty tube, Ψ as a function of the relative density ρ_f/ρ_s of the foam. Predictions are shown in *figure 14* for selected values of the relative strength of the foam to braid (parameterised by σ_c/τ_Y) and for selected ratios of braid radius to wall thickness r/t. For the case shown in *figure 14* the density of the tube wall is taken to be that of GFRP ($\rho_t = 1.8$ Mg/m^3), the initial braid helix angle θ_0 equals 40° and the final braid angle is taken as $\theta_L = 21°$. These values are representative of those used in the experiments on glass fibre braids reported above (Section 3.2).

The normalised energy per unit mass Ψ increases with increasing σ_c/τ_Y for all values of r/t and ρ_f/ρ_s. The maximum value of Ψ occurs at a foam relative density of approximately 0.29, independent of the ratio of crushing strength to shear strength σ_c/τ_Y and of the ratio of radius to wall thickness r/t. This maximum occurs at the point where the lock-up strain switches from that of the braid to that of the foam. The optimal relative density of the foam corresponds to $\varepsilon_r = -\varepsilon_D$, and is given by $\frac{\rho_f}{\rho_s} = 1 - \frac{\sin\theta_L}{2\sin\theta_0}$ from Eqs. (5) and (18).

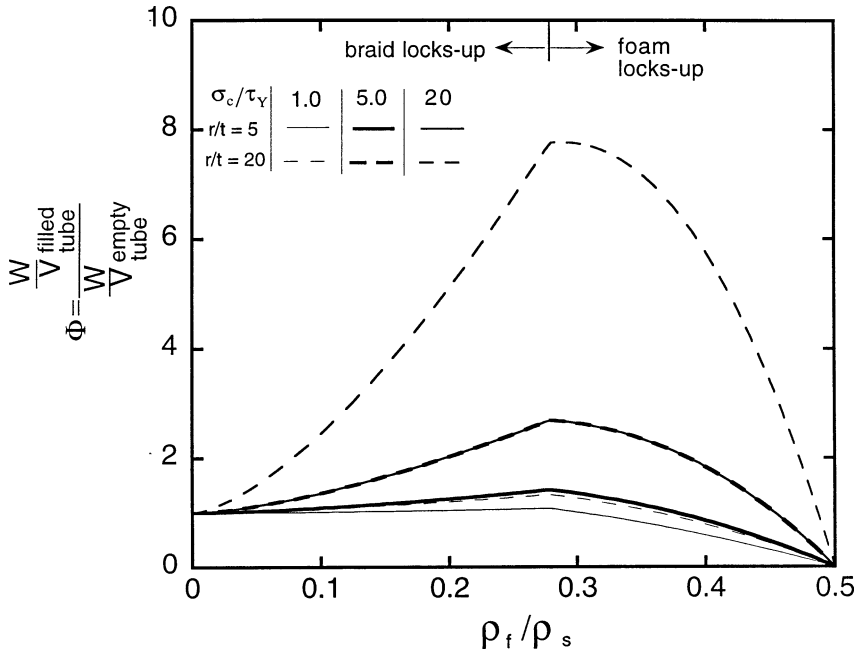

Figure 15. Normalised energy per unit volume of foam-filled tubes in tension, plotted against relative density of foam, for selected ratios of tube radius to wall thickness r/t, and crushing strength of the foam cell walls to matrix shear strength, σ_c/τ_Y.

The prediction (21) for the specific energy absorption W/m and the prediction (23) for the average axial flow stress can be compared with the experimental results shown in *figure 7*. In all experiments a polyurethane foam core of density $\rho_f = 160$ kg/m^3 was employed. The material properties required for the predicted energy absorption were measured independently, and are listed in *table I*. The shear strength of the matrix τ_Y was deduced from a tension test on a $\pm 45°$ braid (see Harte and Fleck, 1999b). For the case of a dry braid, with no epoxy matrix, the predicted energy per unit mass equals 12.5 kJ/kg and the average axial stress is 7.25 MPa, compared with measured values of 5.0 kJ/kg and 6.01 respectively. The measured and predicted energy absorption for the foam-filled glass/epoxy braid are as follows. The measured energy absorption is 5.8 kJ/kg and the average axial stress equals 9.57 MPa for $\theta_0 = 40°$, whereas the predicted values are 11.7 kJ/kg and 11.5 MPa. For the foam-filled glass/epoxy braid with $\theta_0 = 55°$ the predicted values of 18.0 kJ/kg and 5.52 MPa are in acceptable agreement with the experimental values of 10.4 kJ/kg and 4.29 MPa, respectively. The theoretical predictions for the glass/epoxy braids consistently exceed the measured values: a plausible explanation is the fact that the flow strength of the glass/epoxy braid at large plastic strains may be significantly less than the initial yield value due to progressive microcracking of the epoxy matrix between the glass fibres.

When the available volume for an energy absorber imposes a greater limitation on a design than the mass of the energy absorber, it becomes important to optimise the energy per unit volume W/V, where $V = \pi r^2 \ell$ is the volume of the filled tube. The energy per unit volume follows immediately from (20) as

$$\frac{W}{V} = \left(\frac{\cos 2\theta^* - \cos 2\theta_0}{\sin 2\theta_0} \right) \frac{2t}{r} \tau_Y + 2\sigma_{pl} \varepsilon_r^*. \tag{24}$$

The energy per unit volume, normalised by the value for an empty tube, Φ, is plotted against relative density in *figure 15*. The value of Φ increases with increasing σ_c/τ_Y and r/t. A peak value occurs at $\rho_f/\rho_s = 0.29$, corresponding to a switch in the lock-up condition from that of the braid to that of the core.

6. Concluding remarks

Foam-filled braided tubes have been tested in compression and tension and their energy absorbing capabilities have been examined. Approximate analytical models for the energy absorption per unit mass W/m and for the energy absorption per unit volume W/V have been developed.

The foam-filled glass/epoxy tubes tested in the current study failed in compression by axisymmetric plastic buckling of the braided tube walls, with uniaxial crushing of the foam core. The predicted energy absorbed per unit mass W/m and the energy absorbed per unit volume W/V peak when the relative density of the foam core ρ_f/ρ_s equals 0.2 and 0.3, respectively. The effects of the tube radius to wall thickness ratio r/t and the yield strength of the tube wall in relation to the foam cell wall strength σ_c/Y were also addressed. These two non-dimensional groups hardly affect the value of the optimal density but the energy absorbed per unit mass increases with increasing r/t and σ_c/Y.

Acknowledgements

The authors wish to thank the Natural Sciences and Engineering Research Council of Canada, the Newton Trust, and the US Office of Naval Research through the grant number N0014-91-J-1916 for their financial support, and Cambridge Consultants Ltd. for the provision of test materials.

References

Abramowicz W., Wierzbicki T., 1988. Axial crushing of foam-filled columns. Int. J. Mech. Sci. 30 (3/4), 263–271.

Al-Hassani S.T.S., Johnson W., Lowe W.T., 1972. Characteristics of inversion tubes under axial loading. J. Mech. Eng. Sci. 14 (6), 370–381.

Alexander J.M., 1960. An approximate analysis of the collapse of thin cylindrical shells under axial loading. Quart. J. Mech. Appl. Math. 13, 10–15.

Andrews K.R.F., England G.L., Ghani E., 1983. Classification of the axial collapse of cylindrical tubes under quasi-static loading. Int. J. Mech. Sci. 25 (9/10), 687–696.

Barrett J., 1996. Al energy absorber challenges steel. Eureka, 26–27.

Chiu C.H., Tsai K.-H., Huang W.J., 1998. Effects of braiding parameters of energy absorption capability of triaxially braided tubes. J. Comp. Mater. 32 (21), 1964–1983.

Cronkhite J.D., 1984. Design of helicopter composite structures for crashworthiness. Presented at the 5th. International SAMPE Technical Symposium — Design and Use of Kevlar Aramid Fiber in Composite Structures, Reno, Nevada.

Gibson L.J., Ashby M.F., 1997. Cellular Solids. Cambridge University Press.

Hamada H., Ramakrishna S., Nakamura M., Maekawa Z., Hull D., 1994. Progressive crush behaviour of glass/epoxy composite tubes with different surface treatment. Composites Interfaces 2, 127–142.

Hanssen A.G., Langseth M., Hopperstad O.S., 1999. Static crushing of square aluminium extrusions with aluminium foam filler. Int. J. Mech. Sci. 41, 967–993.

Harte A.-M., 1997. The mechanics of braided composites. PhD thesis, Cambridge University Engineering Dept.

Harte A.-M., Fleck N.A., 1999a. Deformation and failure mechanisms of braided composites tubes in compression on torsion. To appear in Acta Materialia.

Harte A.-M., Fleck N.A., 1999b. On the mechanics of braided composites in tension. To appear in Eur. J. Mech. A.

Haug E., De Rouvray, A., 1993. Crash Response of Composite Structures. Structural Crashworthiness and Failure. Elsevier Science Publishers Ltd.

Hull D., 1983. Axial Crushing of Fibre Reinforced Composite Tubes. Structural Crashworthiness, Butterworth and Co Ltd.

Hutchinson J.W., 1974. Plastic Buckling. Adv. in Appl. Mech. 14, 67–144.

Johnson W., Soden P.D., Al-Hassini S.T.S., 1977. Inextensional collapse of thin-walled tubes under axial compression. J. Strain Anal. 12 (4), 317–330.

Karbhari V.M., Falzon P.J., Herzberg I., 1997. Energy absorption characteristics of hybrid braided composite tubes. J. Comp. Mater. 31 (12), 1164–1186.

Kindervater C.M., Georgi H., 1993. Composite Strength and Energy Absorption as an Aspect of Structural Crash Resistance, Structural Crashworthiness and Failure. Elsevier Science Publishers Ltd.

Langseth M., Hopperstad O.S., Hanssen A.G., 1998. Crash behaviour of thin-walled aluminium members. Thin-Walled Structures 32, 127–150.

Mamalis A.G., Manolakos D.E., Viegelahn G.L., Johnson W., 1989. Energy absorption and deformation modes of thin PVC tubes internally grooved when subjected to axial plastic collapse. Proc. Inst. Mech. Engrs. 203, 1–8.

Mamalis A.G., Manolakos D.E., Viegelahn G.L., Vaxevanidis N.M., Johnson W., 1986. The inextensional collapse of grooved thin-walled cylinders of PVC under axial loading. Int. J. Impact Engng. 4, 41–56.

Mikkelsen L.P., 1999. A numerical axisymmetric collapse analysis of viscoplastic cylindrical shells under axial compression. Int. J. Solids and Structures 36, 643–668.

Puglsey A., 1960. The crumpling of tubular structures under impact conditions. In: Proc. of the Symposium on the Use of Aluminium in Railway Rolling Stock, Institute of Locomotive Engineers, The Aluminium Development Association, London, pp. 22–41.

Pugsley A., Macaulay M., 1960. The large-scale crumpling of thin cylindrical columns. Quart. J. Mech. Appl. Math. 13, 1–9.

Reddy T.Y., Wall R.J., 1988. Axial compression of foam-filled thin-walled circular tubes. Int. J. Impact Engng. 7 (2), 151–166.

Reid S.R., Reddy T.Y., Gray M.D., 1986. Static and dynamic axial crushing of foam-filled sheet metal tubes, Int. J. Mech. Sci. 28 (5), 295–322.

Thornton P. H., 1979. Energy absorption in composite structures. J. Compos. Mater. 13, 247–262.

Timoshenko S.P., Gere J.M., 1961. Theory of Elastic Stability. McGraw-Hill Book Company, Inc.

Tvergaard V., 1983. On the transition from a diamond mode to an axisymmetric mode of collapse in cylindrical shells. Int. J. Solids Structures 19 (10), 845–856.

Weingarten V.I., Seide P., Peterson J.P., 1968. Buckling of thin-walled circular cylinders. NASA Space Vehicle Design Criteria, National Aeronautics and Space Administration, Report No. NASA SP-8007.

Wierzbicki T., Bath S.U., Abramowicz W., Brodkin B., 1992. Alexander revisited—a two folding elements model of progressive crushing of tubes. Int. J. Solids Structures 29 (24), 3269–3288.